Supplementary Information

Alternatively spliced mini-exon B in PTPδ regulates excitatory synapses through cell-type-specific trans-synaptic PTPδ-IL1RAP interaction

Seoyeong Kim [1,2,#], Jae Jin Shin [2,#], Muwon Kang [1,2,#], Yeji Yang [1,3], Yi Sul Cho [4], Hyojung Paik [5], Jimin Kim [5], Yunho Yi [1], Suho Lee [2], Hei Yeun Koo [6], Jinwoong Bok [6], Yong Chul Bae [4], Jin Young Kim [3], Eunjoon Kim [1,2,*]

[1]Department of Biological Sciences, Korea Advanced Institute for Science and Technology (KAIST), Daejeon, 34141, Korea; [2]Center for Synaptic Brain Dysfunctions, Institute for Basic Science (IBS), Daejeon, 34141, Korea; [3]Digital Omics Research Center, Korea Basic Science Institute (KBSI), Ochang, 28119, Korea; [4]Department of Anatomy and Neurobiology, School of Dentistry, Kyungpook National University, Daegu, 41940, Korea; [5]Center for Biomedical Computing, Korea Institute of Science and Technology Information (KISTI), Daejeon 34141, Korea; [6]Department of Anatomy, Yonsei University College of Medicine, Seoul, 03722, Korea; [#]These authors contributed equally to the work; *Corresponding author (email: kime@kaist.ac.kr).

Supplementary figures and legends

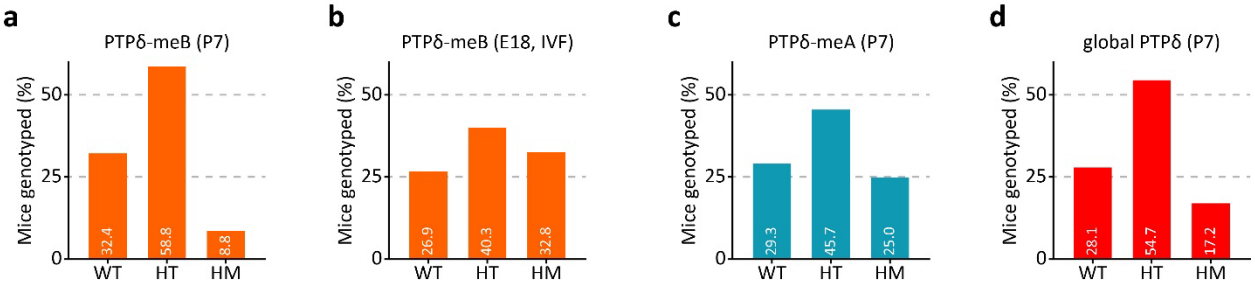

Supplementary Figure 1. Mouse genotype ratios in global PTPδ-mutant, PTPδ-meA-mutant, and PTPδ-meB-mutant mice.

(a–d) Pup or embryo genotype ratios in PTPδ-meB-mutant, PTPδ-meA-mutant, and global PTPδ-mutant mice (WT, wild-type : HT, heterozygote : HM, homozygote) at postnatal day 7 (P7) and PTPδ-meB-mutant mice at embryonic day 18 (E18). E18 embryos were generated through *in vitro* fertilization (IVF). Note that impaired survival is stronger in the order of *Ptprd-meB*$^{-/-}$, *Ptprd*$^{-/-}$ (HM global PTPδ-mutant), and *Ptprd-meA*$^{-/-}$ mice. (n = 102 mice [PTPδ-meB (P7)], 67 [PTPδ-meB (E18, IVF)], 116 [PTPδ-meA (P7)], and 128 [global PTPδ (P7)]; percentage (%) of each genotype is marked on the plot).

Source data are provided as a Source Data file.

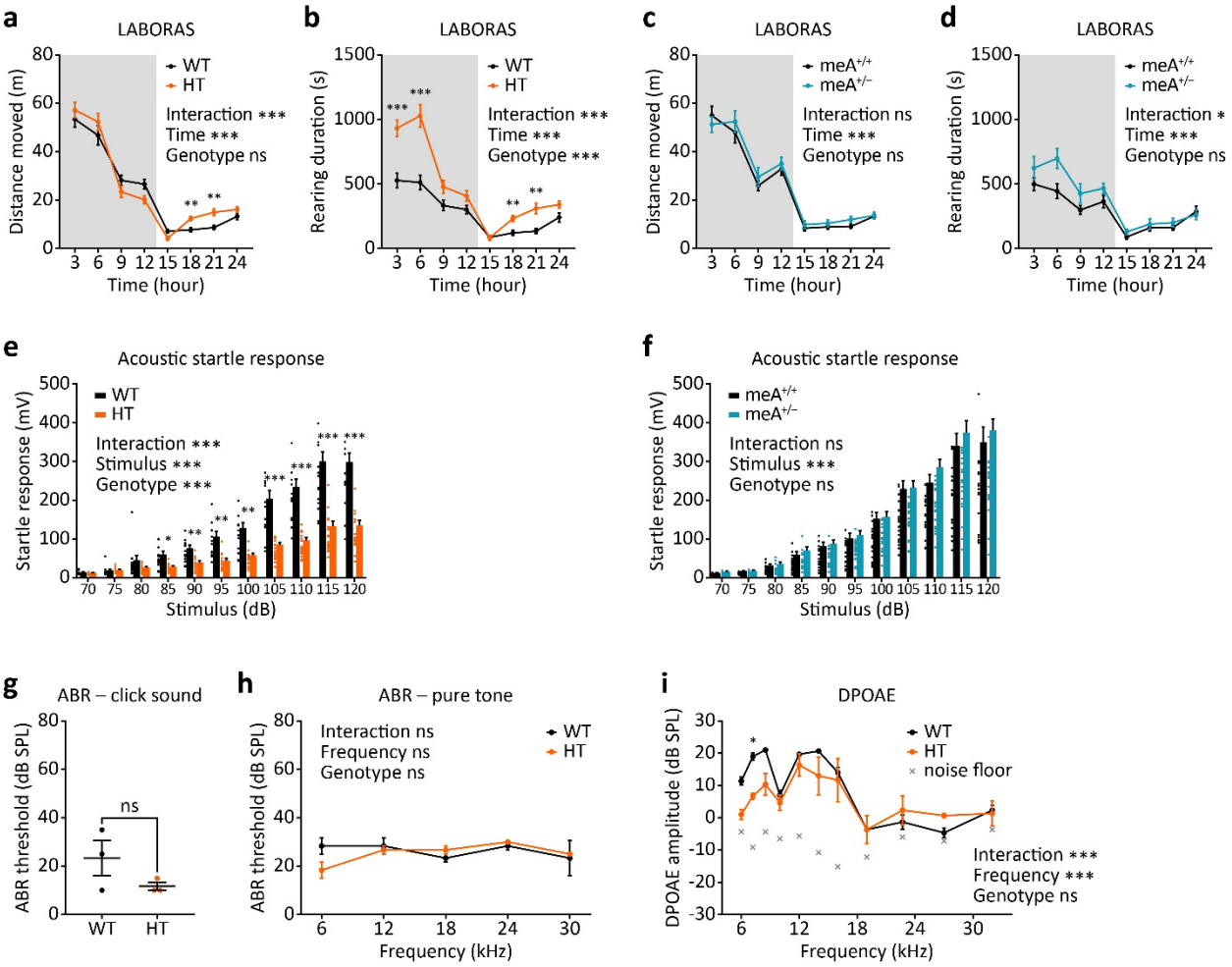

Supplementary Figure 2. Behavioral abnormalities of *Ptprd-meB*$^{+/-}$ mice in LABORAS and acoustic startle response tests.

(a–d) Increased repetitive rearing but largely normal locomotor activity of *Ptprd-meB*$^{+/-}$ mice (P56–84; male) in the LABORAS test. Note that these behaviors are largely normal in *Ptprd-meA*$^{+/-}$ mice (P56–84; male). (n = 19 mice [*Ptprd-meB*$^{+/+}$ (WT)], 20 [*Ptprd-meB*$^{+/-}$ (HT)], 11 [*Ptprd-meA*$^{+/+}$ (meA$^{+/+}$)], 11 [*Ptprd-meA*$^{+/-}$ (meA$^{+/-}$)] for locomotor activity; n = 19 [WT], 20 [HT], 11 [meA$^{+/+}$], 11 [meA$^{+/-}$] for rearing duration, two-way ANOVA with Holm-Sidak's test).

(e–f) Decreased acoustic startle in *Ptprd-meB*$^{+/-}$ but not *Ptprd-meA*$^{+/-}$ mice (P56–84; male). (n = 14 [WT], 18 [HT], 17 [meA$^{+/+}$], 17 [meA$^{+/-}$], two-way ANOVA with Holm-Sidak's test).

(g-i) Normal baseline auditory function in *Ptprd-meB*$^{+/-}$ mice (P63; male), as shown by ABR (auditory brainstem response) threshold and DPOAE (distortion product otoacoustic emissions) amplitude (n = 3 [WT], 3 [HT], two-tailed Student's t-test and two-way ANOVA with Holm-Sidak's test). SPL, sound pressure level;
Data values represent means ± SEM. Significance is indicated as * (< 0.05), ** (< 0.01), *** (< 0.001), or ns (not significant). Source data are provided as a Source Data file.

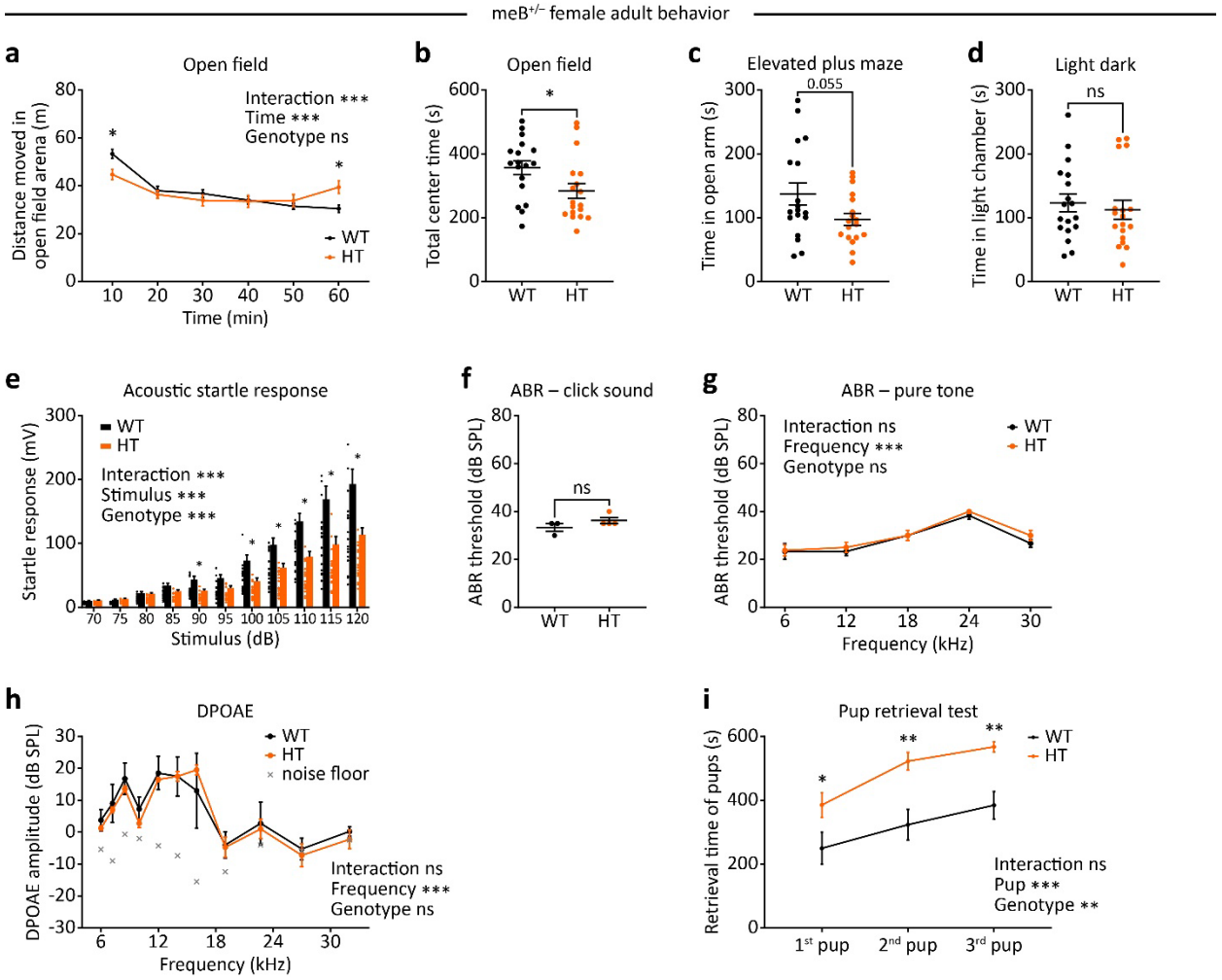

Supplementary Figure 3. Behavioral abnormalities in female *Ptprd-meB*$^{+/-}$ mice.

(a) Hypoactivity of female *Ptprd-meB*$^{+/-}$ mice (P56–84) in the open-field test (first 10 min). (n = 18 mice [WT], 18 [HT], two-way ANOVA with Holm-Sidak's test).

(b) Anxiety-like behavior of female *Ptprd-meB*$^{+/-}$ mice (P56–84) in the open-field test, as shown by time spent in the center region of the open-field cage. (n = 18 [WT], 18 [HT], two-tailed Mann–Whitney test).

(c) Normal anxiety-like behavior of female *Ptprd-meB*$^{+/-}$ mice (P56–84) in the elevated plus-maze test, as shown by time spent in open arms. Note the strong tendency (p = 0.055) towards anxiety-like behavior in the mutant mice. (n = 18 [WT], 18 [HT], two-tailed Welch's t-test).

(d) Normal anxiety-like of female *Ptprd-meB*$^{+/-}$ mice (P56–84) in the light-dark test, as shown by time spent in light box. (n = 18 [WT], 18 [HT], two-tailed Mann-Whitney test).
(e) Decreased acoustic startle in female *Ptprd-meB*$^{+/-}$ mice (P56–84). (n = 18 [WT], 18 [HT], two-way ANOVA with Holm-Sidak's test).
(f–h) Normal baseline auditory functions in female *Ptprd-meB*$^{+/-}$ mice (P63), as shown by ABR threshold and DPOAE amplitude. (n = 3 [WT-ABR], 4 [HT-ABR], 4 [WT-DPOAE], 4 [HT-DPOAE], two-tailed Mann-Whitney test and two-way ANOVA with Holm-Sidak's test).
(i) Decreased pup-retrieval behavior in female *Ptprd-meB*$^{+/-}$ mice (P56–84), as shown by time taken to retrieve all three pups. (n = 18 [WT], 18 [HT], two-way ANOVA with Holm-Sidak's test).
Data values represent means ± SEM. Significance is indicated as * (< 0.05), ** (< 0.01), *** (< 0.001), or ns (not significant). Source data are provided as a Source Data file.

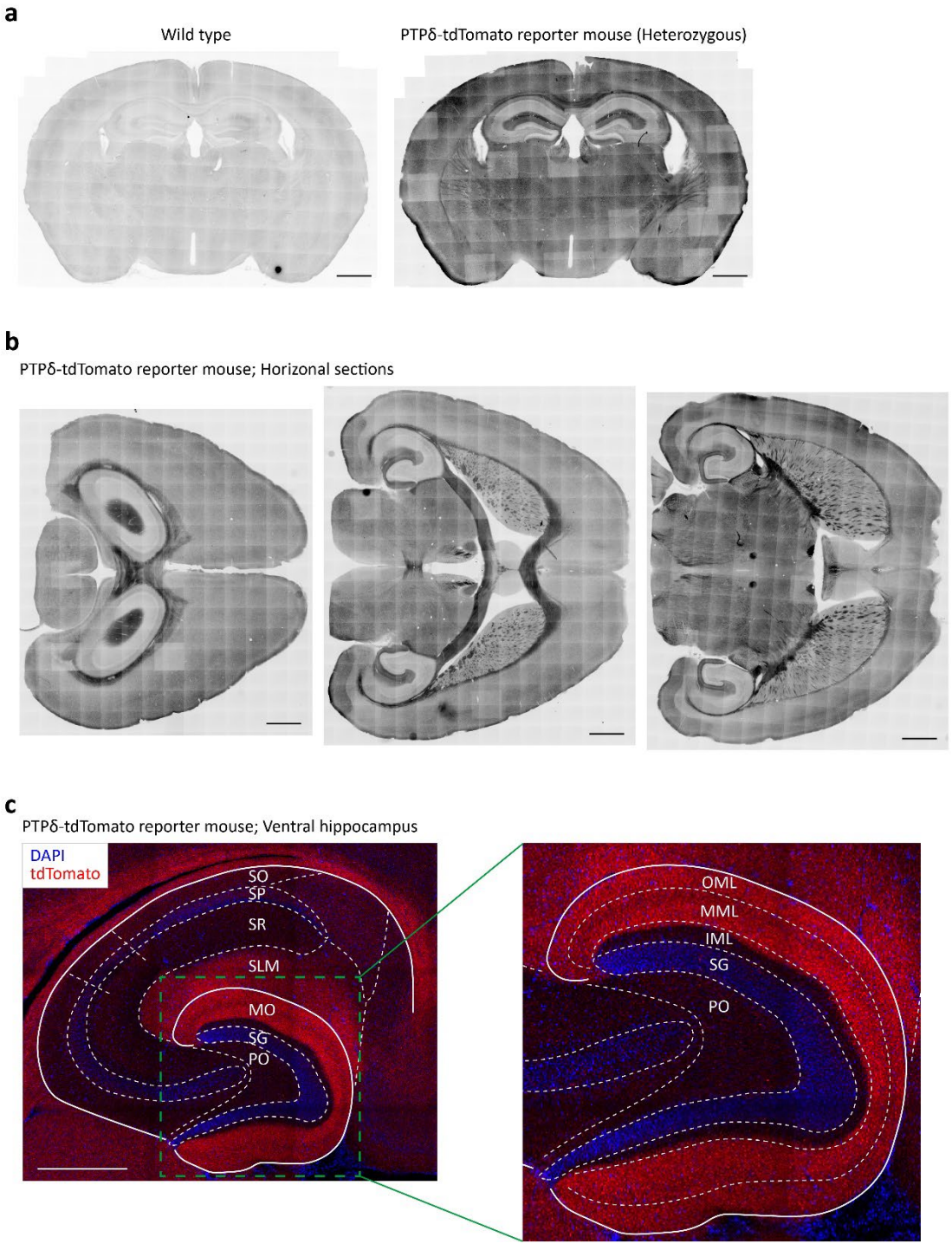

Supplementary Figure 4. PTPδ-tdTomato proteins are detected in the middle and outer molecular layers of the dentate gyrus.

(a) Representative images of PTPδ-tdTomato fusion-protein signal in brain sections from heterozygous PTPδ-tdTomato reporter mice, and a negative-control image from a

WT mouse (P63; male). The red-colored tdTomato signals were converted to grayscale to improve visibility. Scale bar, 1 mm. (n = 2 independent experiments using 2 [Wild type], 2 [PTPδ-tdTomato reporter]).

(b) Horizontal brain sections from heterozygous PTPδ-tdTomato reporter mice (P63; male) revealing tdTomato protein signals in various brain regions. Scale bar, 1 mm. (n = 2 independent experiments using 2 [PTPδ-tdTomato reporter]).

(c) Ventral hippocampus from heterozygous PTPδ-tdTomato reporter mouse (P63; male) showing strong PTPδ-tdTomato signals (red) in the middle molecular layer (MML) and outer molecular layer (OML), which receive synaptic inputs from the medial and lateral entorhinal cortices, respectively. The blue signals represent DAPI staining. SO, stratum oriens; SP, stratum pyramidale; SR, stratum radiatum; SLM, stratum lacunosum moleculare; MO, molecular layer; SG, granule cell layer; PO, polymorphic layer; IML, inner molecular layer; MML, middle molecular layer; OML, outer molecular layer. Scale bar, 500 μm. (n = 2 independent experiments using 2 [PTPδ-tdTomato reporter]).

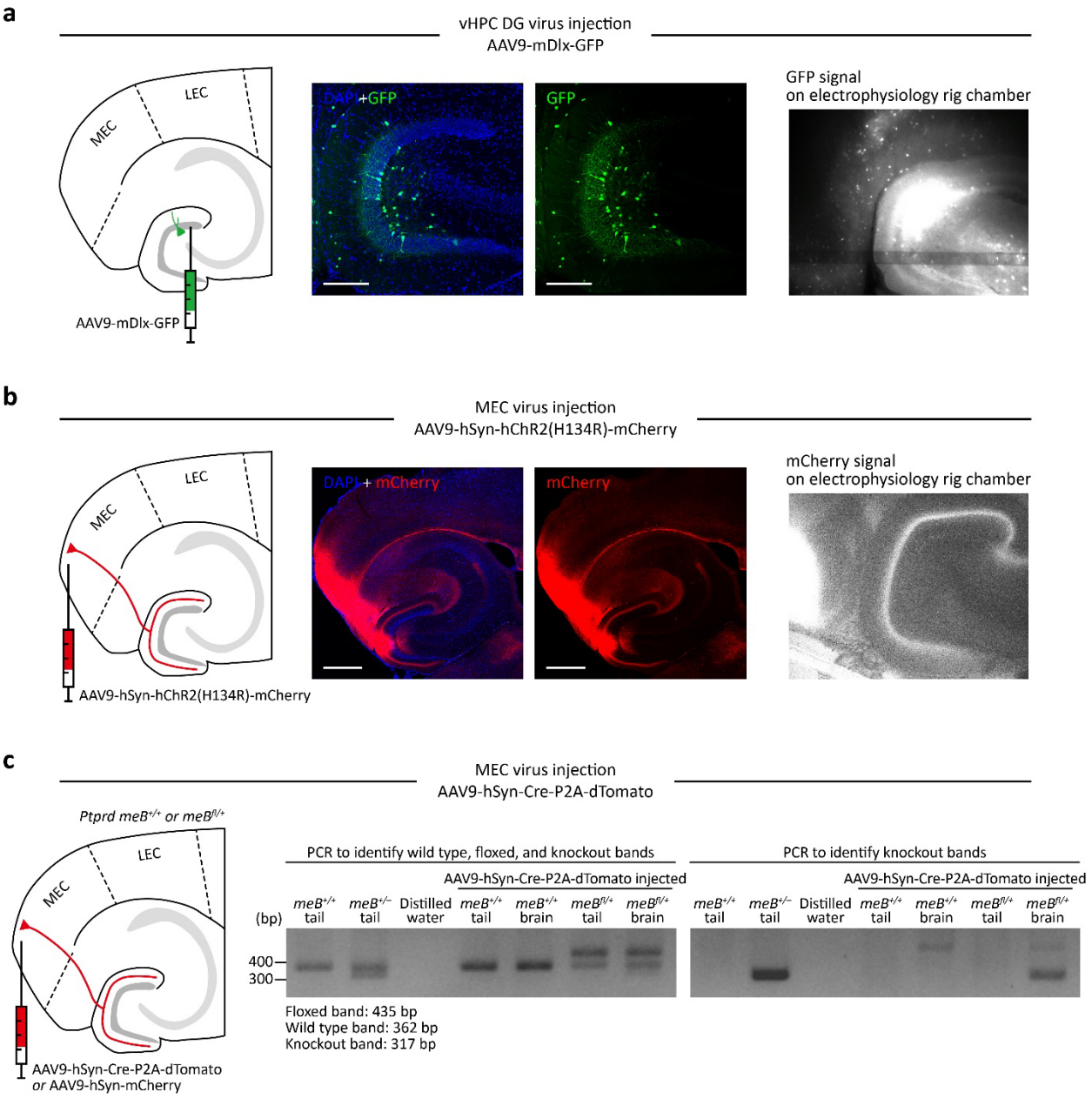

Supplementary Figure 5. Example images for AAV-dependent expression of cell-type-specific markers or neuro-modulatory proteins and confirmation of Cre-dependent *Ptprd-meB* deletion.

(a) Visualization of DG interneurons by injection of AAV9-mDlx-GFP in the dentate gyrus for electrophysiological recordings. Scale bar, 200 μm.

(b) Visualization of DG-projecting entorhinal cortical neurons by injection of AAV9-hSyn-hChR2(H134R)-mCherry in the medial entorhinal cortex (MEC). LEC, lateral entorhinal cortex. Scale bar, 500 μm.
(c) PCR confirmation for conditional deletion of *Ptprd-meB* in the medial entorhinal cortex.

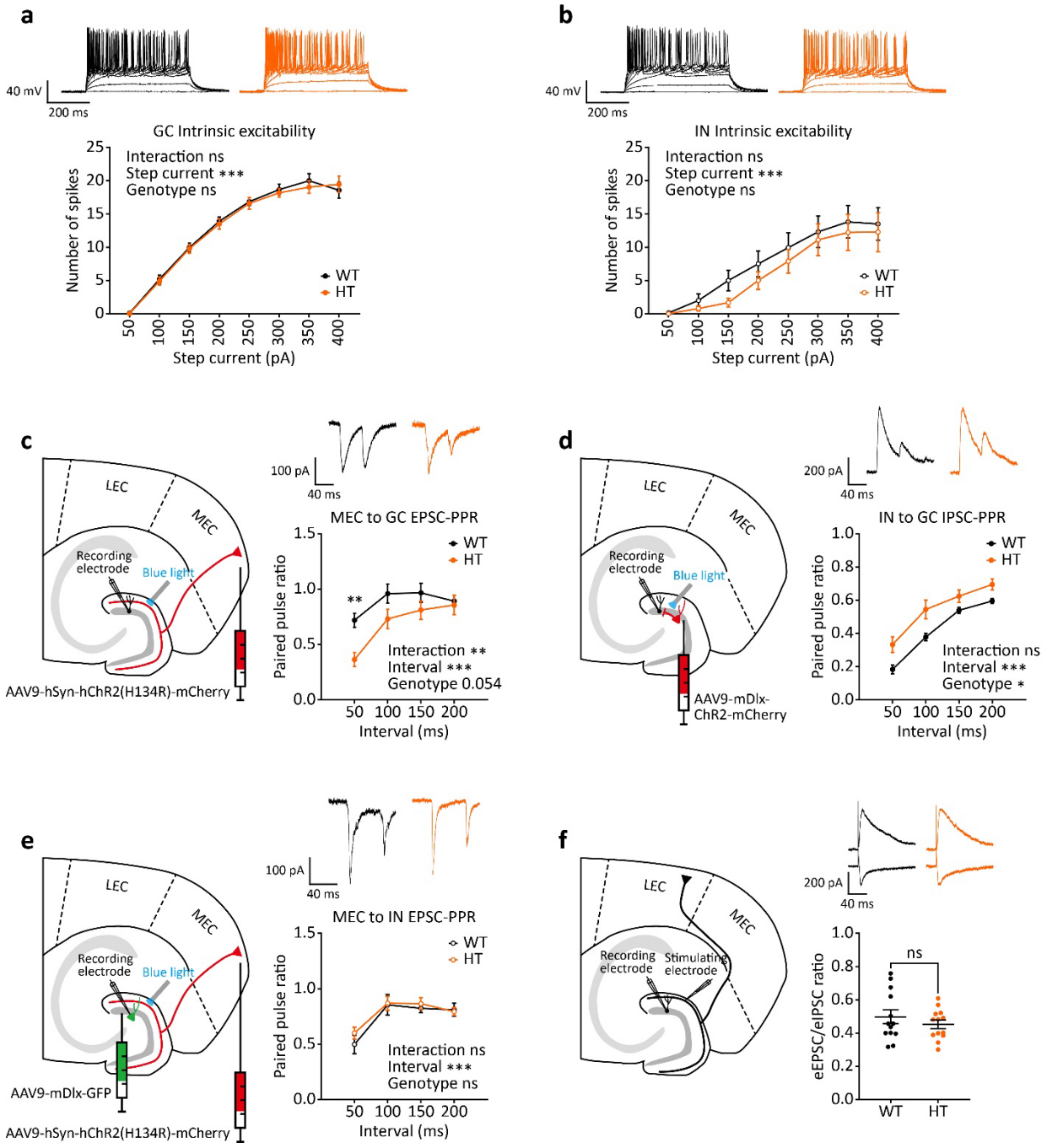

Supplementary Figure 6. Neuronal excitability and paired pulse ratios in DG-GCs and DG-INs, and eEPSC/eIPSC ratios in LEC-DG-GCs.

(a) Normal excitability of *Ptprd-meB*$^{+/-}$ DG-GCs (P56–70; male). (n = 21 neurons from 5 mice [WT], 22, 6 [HT], two-way ANOVA with Holm-Sidak's test).

(b) Normal excitability of *Ptprd-meB*$^{+/-}$ DG-INs (P56–70; male). (n = 16, 6 [WT], 18, 7 [HT], two-way ANOVA with Holm-Sidak's test).
(c) Decreased EPSC paired-pulse ratios (PPRs) in the MEC to DG-GC pathway (P56–70; male) of *Ptprd-meB*$^{+/-}$ mice infected with AAV9-hSyn-hChR2(H134R)-mCherry in the MEC. (n = 15, 5 [WT], 13, 5 [HT], two-way ANOVA with Holm-Sidak's test).
(d) Increased IPSC PPRs in the DG-IN to DG-GC pathway (P56–70; male) of *Ptprd-meB*$^{+/-}$ mice infected with AAV9-mDlx-ChR2-mCherry in the DG. (n = 9, 2 [WT], 9, 2 [HT], two-way ANOVA with Holm-Sidak's test).
(e) Normal EPSC PPRs in the MEC to DG-IN pathway (P56–70; male) of *Ptprd-meB*$^{+/-}$ mice infected with AAV9-mDlx-GFP in the DG (to mark DG-INs) and infected with AAV9-hSyn-hChR2(H134R)-mCherry in the MEC (to stimulate the pathway). (n = 7, 4 [WT], 10, 3 [HT], two-way ANOVA with Holm-Sidak's test).
(f) Normal eEPSC/eIPSC ratios in *Ptprd-meB*$^{+/-}$ DG-GCs in the LEC-DG pathway (P56–70; male). (n = 13,3 [WT], 13, 3 [HT], two-tailed Student's t-test).
Data values represent means ± SEM. Significance is indicated as * (< 0.05), ** (< 0.01), *** (< 0.001), or ns (not significant). Source data are provided as a Source Data file.

a

Protein name	PSD fraction			SPM fraction			Whole lysate		
	P-value	Fold change	Significance (Y/N)	P-value	Fold change	Significance (Y/N)	P-value	Fold change	Significance (Y/N)
IL1RAP	0.0346	−1.2020	Y	0.2663	−1.0359	N	0.3968	1.0175	N
IL1RAPL1	ND	ND	-	0.0004	−1.1649	N	0.7326	−1.0160	N
LRFN4 (SALM3)	ND	ND	-	0.9128	1.0063	N	0.3467	1.0592	N
LRFN5 (SALM5)	ND	ND	-	0.0270	1.0729	N	0.1183	−1.0684	N
NLGN3	0.6262	−1.7815	N	0.4463	1.0238	N	0.6381	1.0143	N
SLITRK1	ND	ND	-	0.0013	−1.0444	N	0.7453	1.0235	N
SLITRK2	ND	ND	-	0.0273	1.0493	N	0.0322	1.0695	N
SLITRK3	ND	ND	-	0.0016	1.1788	N	0.1083	1.0936	N
SLITRK4	ND	ND	-	0.3613	1.0264	N	0.3813	1.0449	N
SLITRK5	ND	ND	-	0.7993	−1.0050	N	0.0347	1.1017	N
PTPδ	0.2036	1.0973	N	0.0017	1.1103	N	0.0923	1.0545	N
PTPσ	0.9244	−1.0090	N	0.0694	−1.0690	N	0.8503	−1.0026	N
LAR	0.2220	1.1503	N	0.9223	1.0014	N	0.2455	−1.0397	N

Supplementary Figure 7. A preferential decrease of IL1RAP in the PSD fraction of *Ptprd-meB*$^{+/-}$ mice revealed by total proteomic analysis

(a) Shown are the levels of PTPδ-binding proteins and PTPδ/PTPσ/LAR family members across three sample types derived from whole brains of P63 male mice (WT and *Ptprd-meB*$^{+/-}$): the postsynaptic density (PSD) fraction, the synaptic plasma membrane (SPM) fraction, and whole lysate. Proteins were deemed significantly differentially expressed (DEPs) if they exhibited a p-value < 0.05 and an absolute fold-change > 1.2. Notably, IL1RAP is the only protein significantly decreased in the PSD fraction (highlighted in blue).

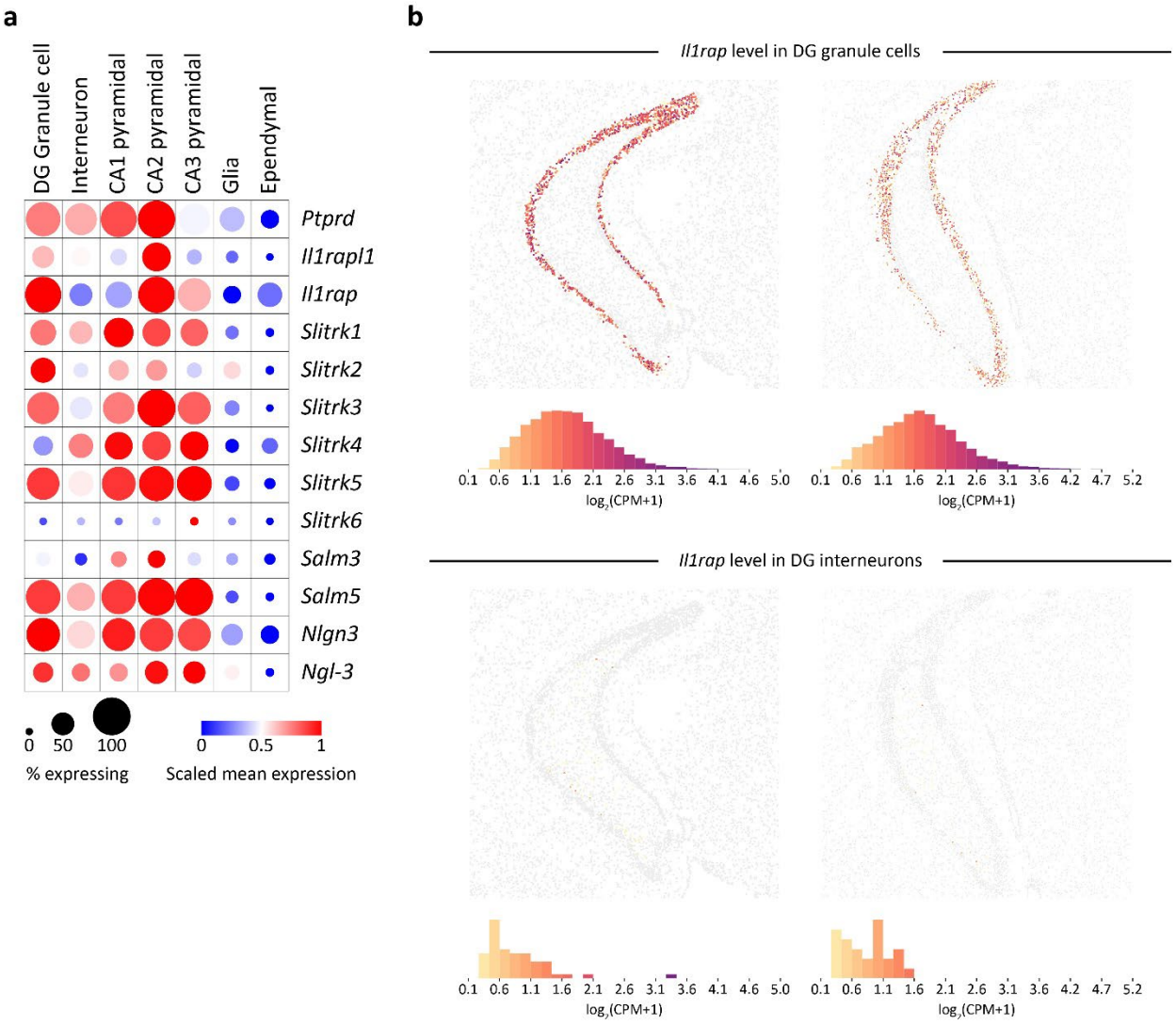

Supplementary Figure 8. mRNA levels of known trans-synaptic partners of PTPδ, including IL1RAP, in the mouse hippocampus.

(a) mRNA levels of known trans-synaptic partners of PTPδ in hippocampal regions of mouse brains (12–16 weeks; male), as determined by analysis of single-nucleus RNA-Seq data from the Broad Institute Single Cell Portal [1,2].

(b) Expression patterns of *Il1rap* mRNAs in the mouse hippocampus (P56–62; male/left and female/right), as determined by analysis of MERFISH data from the Allen Brain Atlas [3,4].

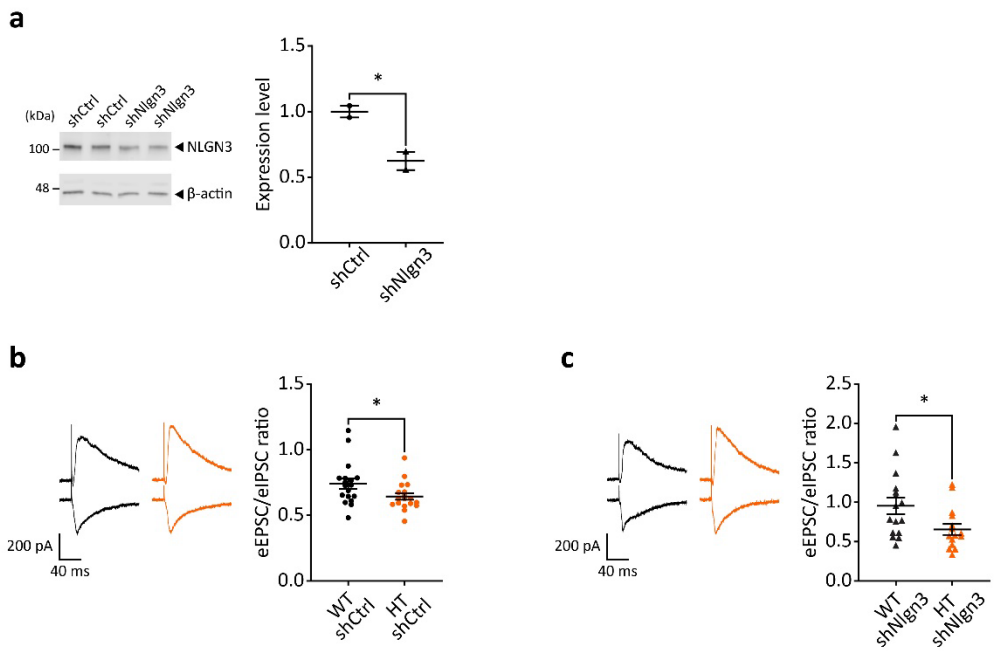

Supplementary Figure 9. Neuroligin-3 protein levels in shRNA-treated cultured hippocampal neurons and eEPSC/eIPSC ratios in shRNA-treated DG-GCs of WT and *Ptprd-meB*$^{+/-}$ mice.

(a) Decreased Neuroligin-3 protein levels in WT cultured hippocampal neurons treated with AAV9-U6-shNlgn3-GFP (virus applied on days in vitro/DIV 7 and harvested on DIV 14). (n = 2 independent cultures [shCtrl, shNlgn3], two-tailed Student's t-test).

(b) Decreased eEPSC/eIPSC ratios in DG-GCs in *Ptprd-meB*$^{+/-}$ mice (P56–70; male) injected with AAV9-U6-shCtrl-GFP in the DG. Note that this result is in line with the decreased eEPSC/eIPSC ratios in naïve DG-GCs in the MEC-DG pathway of *Ptprd-meB*$^{+/-}$ mice. (n = 18 neurons from 4 mice [WT shCtrl], 18, 3 [HT shCtrl], two-tailed Mann–Whitney test).

(c) Decreased eEPSC/eIPSC ratios in DG-GCs in *Ptprd-meB*$^{+/-}$ mice (P56–70; male) injected with AAV9-U6-shNlgn3-GFP in the DG. (n = 16, 3 [WT shNlgn3], 15, 4 [HT shNlgn3], two-tailed Student's t-test). Note that shNlgn3 expression maintains the baseline genotype difference in eEPSC/eIPSC ratios between WT and *Ptprd-meB*$^{+/-}$ mice.

Data values represent means ± SEM. Significance is indicated as * (< 0.05). Source data are provided as a Source Data file.

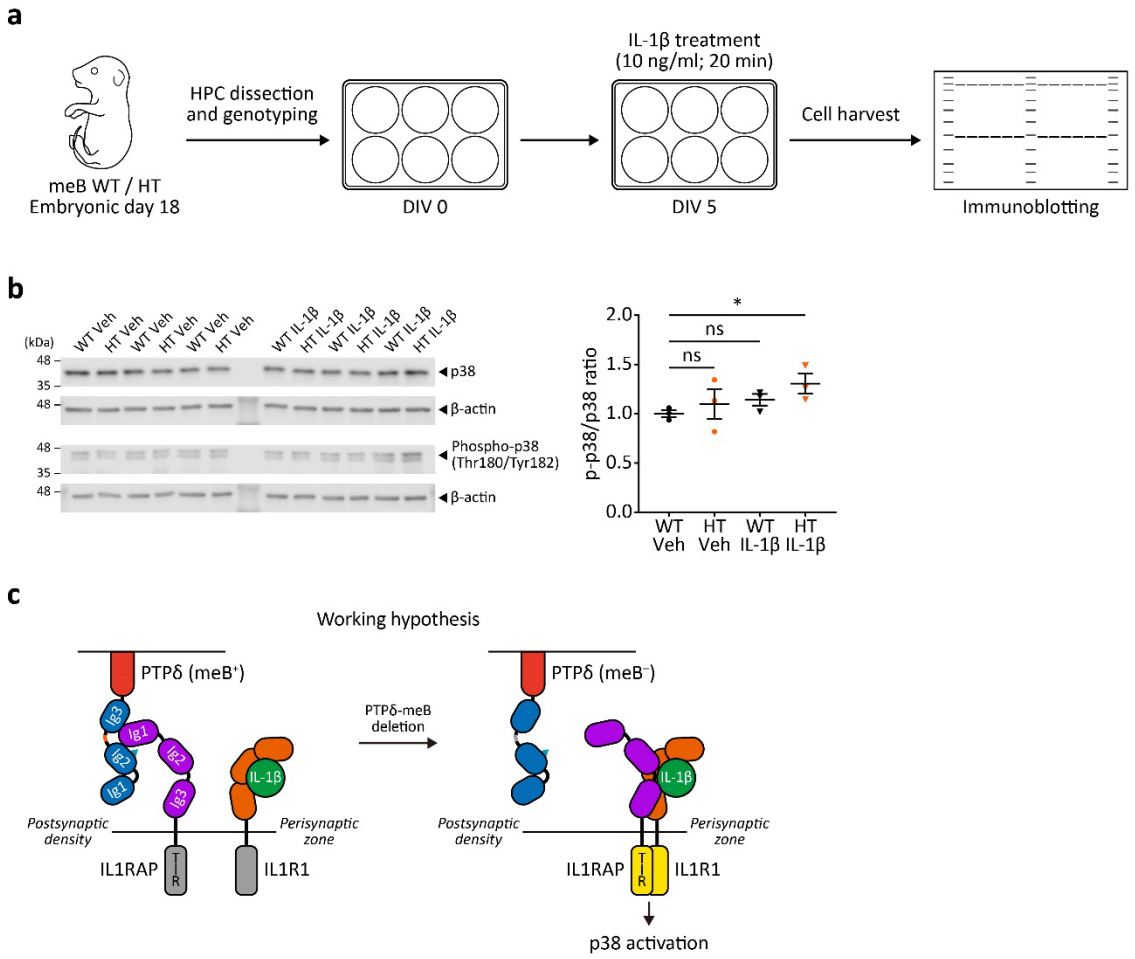

Supplementary Figure 10. Increased p38 activation in IL-1β-treated *Ptprd-meB*$^{+/-}$ cultured hippocampal neurons.

(a) Diagram showing the treatment of *Ptprd-meB*$^{+/-}$ cultured hippocampal (HPC) neurons with IL-1β (10 ng/ml; 20 min) followed by the immunoblotting of total and phosphorylated p38 for assessing the activation of p38.

(b) Immunoblot analysis of total and phosphorylated p38. (n = 3 independent cultures [WT-Veh, HT-Veh, WT-IL-1β, and HT-IL-1β], Student's t-test).

(c) Working hypothesis on how PTPδ-meB deletion enhances IL-1β signaling by suppressing postsynaptic IL1RAP localization. Under normal conditions, the trans-synaptic PTPδ–IL1RAP interaction localizes IL1RAP at the PSD, restricting IL1RAP's interaction with IL-1β-bound IL1R1 and limiting downstream p38 activation. In the absence of PTPδ-meB, however, postsynaptic IL1RAP is released from the PSD,

readily forming a complex with IL-1β-bound IL1R1 and resulting in enhanced p38 activation. Ig, immunoglobulin-like domain; IL-1β, interleukin 1β; IL1R1, interleukin 1 receptor type I; TIR, Toll–IL-1 receptor domain.

Data values represent means ± SEM. Significance is indicated as * (< 0.05) or ns (not significant). Source data are provided as a Source Data file.

Source Data (uncropped gel and blot images for the Supplementary Figures)

Supplementary Figure 5c uncropped images

PCR to identify wild type, floxed, and knockout bands

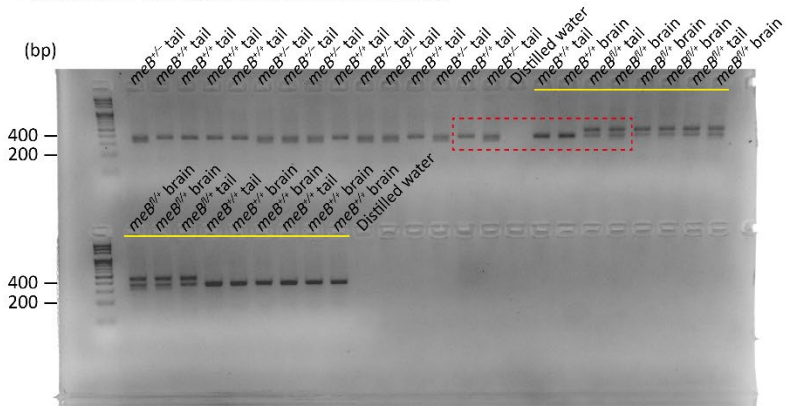

Floxed band: 435 bp
Wild type band: 362 bp
Knockout band: 317 bp

Yellow lines indicate AAV9-hSyn-Cre-P2A-dTomato injected mice

PCR to identify knockout bands

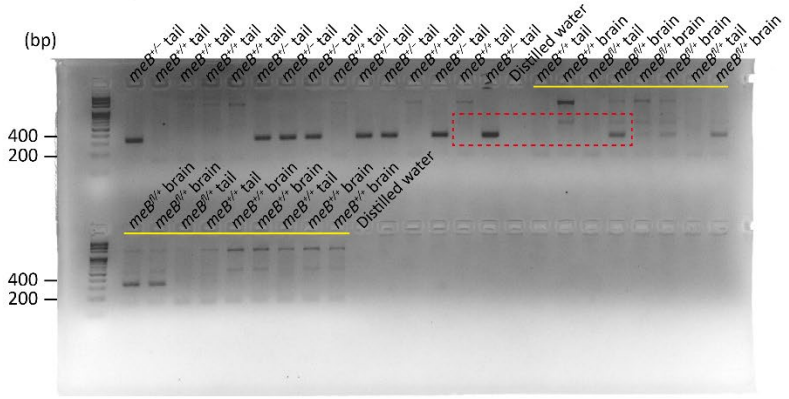

Knockout band: 317 bp

Yellow lines indicate AAV9-hSyn-Cre-P2A-dTomato injected mice

Supplementary Figure 9a uncropped images

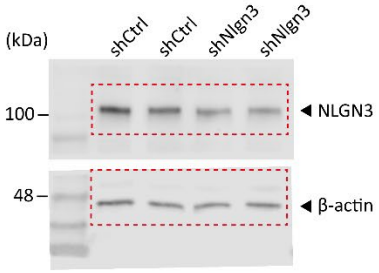

Supplementary Figure 10b uncropped images

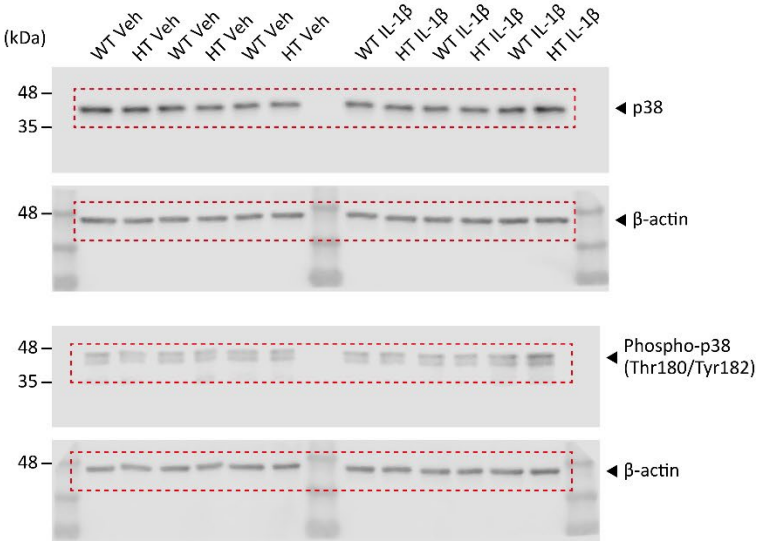

Supplementary references

1. Tarhan, L.*, et al.* Single Cell Portal: an interactive home for single-cell genomics data. *bioRxiv* (2023).
2. Habib, N.*, et al.* Div-Seq: Single-nucleus RNA-Seq reveals dynamics of rare adult newborn neurons. *Science* **353**, 925-928 (2016).
3. Chen, K.H., Boettiger, A.N., Moffitt, J.R., Wang, S. & Zhuang, X. RNA imaging. Spatially resolved, highly multiplexed RNA profiling in single cells. *Science* **348**, aaa6090 (2015).
4. Zhang, M.*, et al.* Molecularly defined and spatially resolved cell atlas of the whole mouse brain. *Nature* **624**, 343-354 (2023).